論文 / 著書情報
Article / Book Information

Title	Study on the hydraulic characteristics of natural levees by field surveys: Case study of the Kokai River, Japan
Authors	Wenyue Zhang, Mai Tabuchi, Tomotaka Yoshikawa, Akihiro Takahashi
Citation	Soils and Foundations, Vol. 65, Issue 5, 101679
Pub. date	2025, 9
DOI	https://doi.org/10.1016/j.sandf.2025.101679
Creative Commons	Information is in the article.

HOSTED BY
ELSEVIER
Available online at www.sciencedirect.com
ScienceDirect
Soils and Foundations 65 (2025) 101679
www.elsevier.com/locate/sandf

Technical Report

Study on the hydraulic characteristics of natural levees by field surveys: Case study of the Kokai River, Japan

Wenyue Zhang [a], Mai Tabuchi [b], Tomotaka Yoshikawa [b], Akihiro Takahashi [b,*]

[a] *Taisei Advanced Center of Technology, Taisei Corporation, Yokohama, Japan*
[b] *Department of Civil and Environmental Engineering, Institute of Science Tokyo, 2-12-1, Oh-okayama, Meguro, Tokyo 152-8550, Japan*

Received 17 January 2025; received in revised form 23 June 2025; accepted 12 August 2025

Abstract

As compensation for the limited experimental data from the borehole logs, geological knowledge is expected to contribute to better risk assessment of the river levee system. Although natural levees have long been recognized as related to the underseepage risk of river levees, limited quantitative knowledge of hydraulic characteristics is available. Field surveys are conducted at a site along the Kokai River in Japan to reveal the hydraulic characteristics of natural levee sediments. Sounding tests allow us to capture laminar structures in the natural levee sediments. Through in-situ seepage tests, it is found that the silty materials in the natural levee sediments have hydraulic conductivity in the order of around E-06 m/s. Based on the results from the field surveys, numerical spatial hydraulic conductivity models of natural levees are built by applying geostatistical methods, including indicator Kriging and indicator simulations. The methodology in this study shows a possibility of quantifying geological knowledge, which finally contributes to the quantitative risk assessment against underseepage and internal erosion.

Keywords: River levees; Natural levees; In-situ test; Underseepage; Geostatistics

1. Introduction

Understanding the soil profiles and the hydraulic characteristics of the river levees is a key step for the risk assessment against underseepage and internal erosion (USACE, 2000, 2005; JICE, 2012). In the Netherlands, baseline values for the risk assessment in a spacing of 2 km along the river can be decided by referring to the WTI-SOS system (Winkels et al., 2021); in Japan, safety against underseepage is checked along the river in a spacing of 1 to 2 km, based on the soil profiles estimated by borehole logs (MLIT, 2007). Although the existing practice generally ensures the safety of the river levee system, a more accurate risk assessment is required, considering the more extreme weather accompanied by climate change and demands for narrowing down the reinforcement segments due to the future lack of labour. It is pointed out that backward erosion piping (BEP) is affected by the heterogeneity in the scale of centimetre to tens of meters (Negrinelli et al., 2016; Liang et al., 2017; Polanco-Boulware & Rice, 2017), the required data for which is infeasible to be provided by traditional borehole drilling. Geophysical surveys, including electrical resistivity tomography (Strange et al., 2016; Martin et al., 2017) and surface-wave methods (Hayashi, 2008), provide continuous information in two dimensions, but their applicability is limited by the ambiguity in interpreting the data and the dilemma in trading off the resolution and the range of the survey. A feasible choice is (1) to use geological knowledge, (2) to extract informa-

* Corresponding author.
E-mail addresses: tu-bne00@pub.taisei.co.jp (W. Zhang), takahashi.a.3a81@m.isct.ac.jp (A. Takahashi).

https://doi.org/10.1016/j.sandf.2025.101679
0038-0806/

tion from the landform classification, and (3) to analogise the hydraulic characteristics of similar alluvial landforms.

Among alluvial landforms, the natural levee is noticeable in Japan (Itsukushima, 2018). During historical floods, suspension loads are deposited on the riverbank, forming elevated structures along the rivers (Brierley & Fryirs, 2005). It has long been raised that these sandy to silty materials provided a seepage path under the river levees, leading to leakages and piping events (River Center of Hokkaido, 2004; Kuroki & Shinagawa, 2018). A statistical study on the levees of 92 river systems in Japan revealed that natural levees are one of the typical landforms susceptible to leakage events (PWRI, 2010). Despite the importance of natural levees, only qualitative knowledge about them is provided by geologists (Brierley et al., 1997; Ferguson & Brierley, 1999), while little quantitative data (Filgueira-Rivera, 2007), especially the data about their hydraulic characteristics, is available.

In this study, the hydraulic characteristics of natural levees are studied by field surveys (1) to attain quantitative data about the hydraulic characteristics of natural levee sediments and (2) to build numerical spatial hydraulic conductivity models for natural levee sediments. By attaining more quantitative knowledge about natural levees, we get closer to the final goal of bridging geological knowledge and the risk assessment of river levees.

2. Methodology

The methodology applied in this study is illustrated in Fig. 1. The concept of the facies model, in which geological clusters called depositional facies have similar properties (Anderson, 1997), is adopted in the study. By conducting sounding tests, soil profiles of the targeted alluvial sediments are retrieved, based on which numerical models of the depositional facies are built by applying geostatistical methods. In-situ seepage tests attain the mean hydraulic conductivity of the corresponding depositional facies. Applying the corresponding mean hydraulic conductivity to the depositional facies, numerical spatial hydraulic conductivity models are built. An advantage of this methodology is that the geological characteristics of the depositional facies can be reflected, rather than simply assuming the log-normal distribution of hydraulic conductivity (Liang et al., 2017; Robbins et al., 2021), which is supported by limited field data (Kanning, 2012) and a lack of geological meaning (Fogg, 1998). Although not covered in this study, as illustrated in dotted lines (Fig. 1), numerical simulations can be conducted on the numerical models, which finally leads to a better assessment of the safety of river levees. Detailed explanations of the sounding tests and the in-situ seepage tests are addressed in the following subsections.

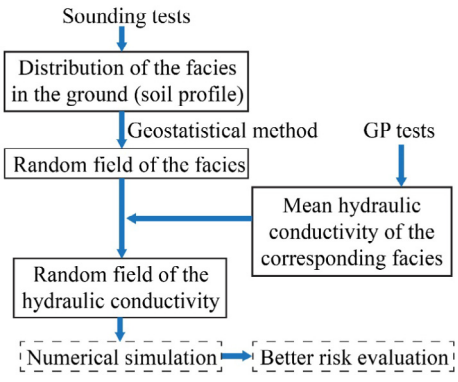

Fig. 1. Illustration of the methodology to integrate the field surveys into risk assessment.

2.1. Sounding tests

A simplified manual sounding test called "handle penetrating stick" is applied in the study (Workshop on the handle penetrating stick, 2023). As shown in Fig. 2, the device comprises a handle, extending rods (diameter $\phi = 10$ mm), and a vane cone at the tip. By pushing the stick into the ground, the penetrating resistance, which is related to the friction angle and the cohesion of the soil, can be measured by a load gauge or subjectively judged by the operator. At specific depths in the ground, a vane shear test can be performed by rotating the rod with a torque wrench without exerting vertical load, by which shear resistance, mainly related to the cohesion of the ground, can be measured. The device applies to a depth within 5 m from the ground surface for the ground with an SPT N value of $10 \sim 15$.

In this study, the handle penetrating stick is applied to grasp the soil profiles qualitatively. During the penetration of the rod with the vane cone on the tip, the penetrating resistance is subjectively judged by the operator at every 5 cm, recorded by five levels: very soft "vs" (the rod can be inserted without feeling much resistance), soft "s" (the rod can be easily inserted by hand), firm "f" (the rod can be inserted by loading the weight of the operator), "h" (the rod can be inserted by hitting the handle forcefully with a rubber hammer), and very hard "vh" (the rod can be hardly inserted even by hitting the handle forcefully with a rubber hammer). A vane shear test is performed at every $10 \sim 20$ cm depth increment during the penetration without exerting a vertical load. By rotating the rod at a constant speed (approximately one rad/s) with a torque wrench, the vane shear resistance (N•m) can be quantitatively measured. An example of the measurement is shown in Fig. 3, in which the classification of depositional facies is defined in Subsection 3.2.

To build a relationship between information from the sounding tests and the classification of soils, the sounding test is calibrated by several trial tests, as illustrated in Fig. 4. Next to the spots where the sounding tests are performed, samples are collected from the auger holes with a diameter of 8 cm, on which visual observation, tactile sense, and grading tests are performed. An example of the calibration is illustrated in Fig. 3. In the shallow portion to the

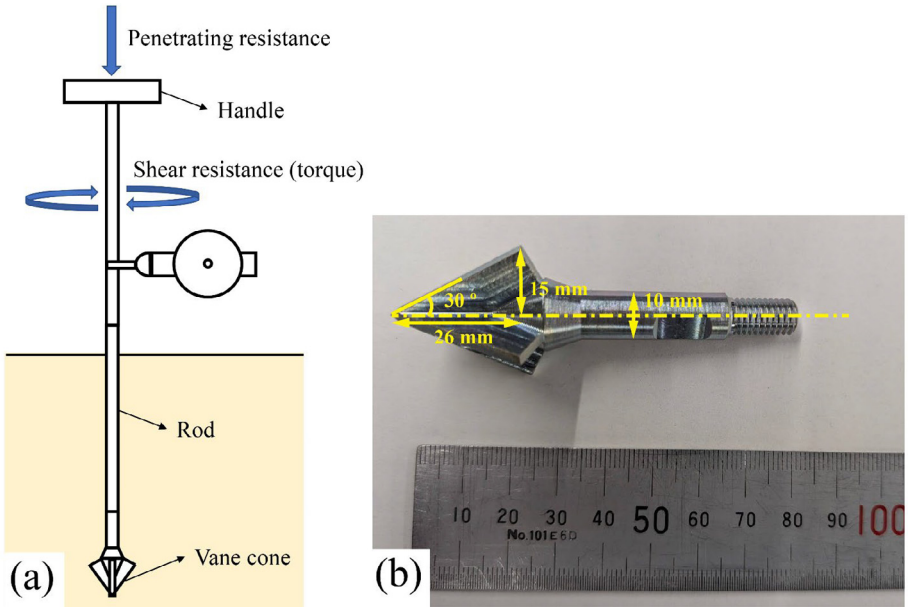

Fig. 2. (a) Schematic sketch of the handle penetrating stick and (b) the dimension of the vane cone.

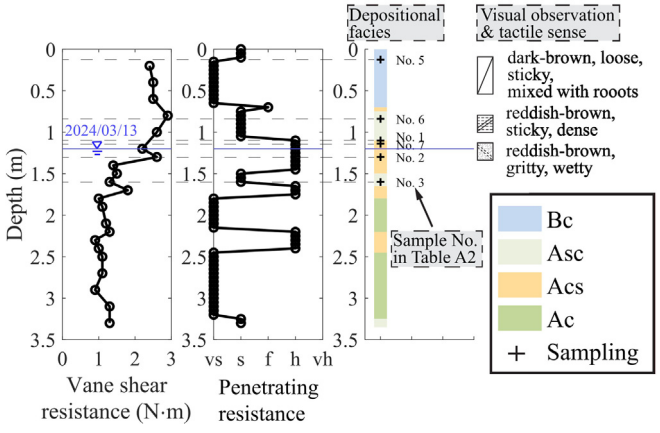

Fig. 3. Measurement at the "o3" spot by the handle penetrating test.

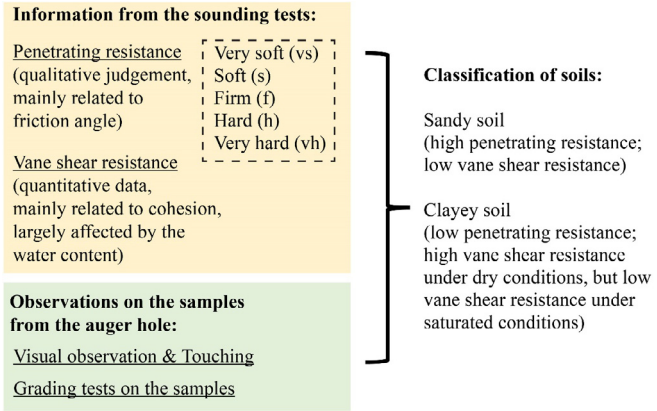

Fig. 4. Method to relate the information from the sounding tests to the classification of soils.

depth of around 0.7 m from the ground surface, the silty surface soil has high vane shear resistance and low penetrating resistance; in the deeper portion at the depth of around 0.8 ~ 1 m, the denser silty soil has high vane shear resistance and relatively low penetrating resistance; at the depth of around 1.1 ~ 1.5 m, gritty materials are met (confirmed by visual observation and tactile sense on the collected samples, and also by the scratching sound heard when digging auger holes), leading to relatively low vane shear resistance and apparently high penetrating resistance; below the water table, possibly due to the high water contents in the cohesive soil, high vane shear resistance is no longer accompanied by low penetrating resistance. The grain size distributions of the samples collected, besides spot "o3", are further discussed in Subsection 3.2. By comparing the results from the several trial tests in different locations, it is concluded that sandy soil generally has high penetrating resistance (firm to very hard) but low vane shear resistance (basically < 2 N•m); clayey soil generally has low penetrating resistance (soft to very soft), while the vane shear resistance is largely affected by the water content of the soil (2 ~ 3 N•m above groundwater level; 1 ~ 2 N•m below the groundwater level). In conclusion, sandy and clayey soil can be generally distinguished by the penetrating resistance, while the vane shear resistance provides additional confirmation. Although error may be introduced in this qualitative relationship, as illustrated in Subsection 3.2, this simple method can satisfactorily capture characteristic laminar structures of the natural levee.

2.2. In-situ seepage tests

Hydraulic conductivity is one of the key factors related to BEP (Kanning, 2012). Although laboratory seepage tests

on disturbed samples are suggested to be performed at the embankment bodies, and in-situ seepage tests are suggested to be performed at the foundations (JICE, 2012), limited experimental data are available in the existing database (Zhang & Takahahsi, 2022). To measure the in-situ hydraulic conductivities of the corresponding depositional facies in the natural levees, it is necessary to have an in-situ seepage test with a proper testing scale, demanding low cost and short testing time. As illustrated in Fig. 5, in the Guelph Permeameter (GP) test, in-situ field saturated hydraulic conductivities K_{fs} (m/s) in the unsaturated zone can be calculated from the steady flow rate Q_s (L/min) out of the reservoir, by keeping a constant head in the auger hole. By applying a set of portable testing device, in-situ field saturated hydraulic conductivities K_{fs} (m/s) along the depth in the unsaturated zone can be measured within several minutes to an hour, requiring only one or two operators (Reynolds & Elrick, 1987; Bagarello et al., 1999; MacDonald et al., 2012; ASTM, 2016). It has been confirmed that the device gives reasonable measurements on the sandy to clayey soil in an alluvial environment, with a representative volume in the scale of several to tens of centimetres (Zhang & Takahashi, 2024).

The GP tests in the field survey are performed in auger holes with a radius $r = 3$ cm, at the depths $H = 0.4 \sim 1.6$ m from the ground surface, with a constant water head $L = 15$ cm during the tests. The field-saturated hydraulic conductivities are calculated using Reynolds' solution (Reynolds, 2013):

$$K_s = \frac{CQ_s}{2\pi L^2 + C\pi r^2 + 2\pi L/\alpha^*} \tag{1}$$

where C is a shape factor, α^* (m^{-1}) is a factor related to the capillarity of soil.

In this study, $\alpha^* = 12\ m^{-1}$ and $C = 1.69$ are applied, as recommended by JGS (2017). Justification for applying the Reynolds' solution with these values can be found in Zhang (2024).

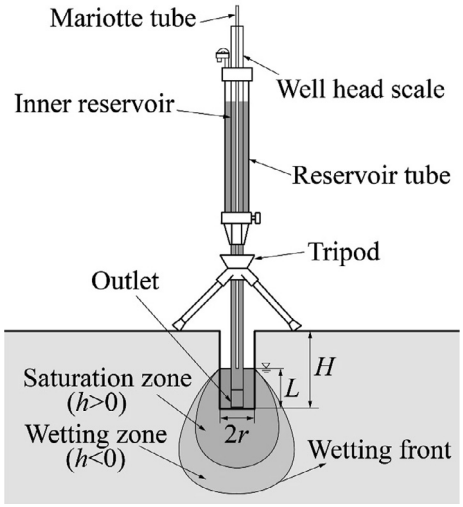

Fig. 5. Illustration of the portable device for the GP test.

2.3. Soil samplings and laboratory seepage tests

To calibrate the sounding tests and to perform the in-situ seepage tests, auger holes are drilled, from which soil samples are collected. Elementary laboratory tests, including tests for the density of soil particles and tests for the particle size distribution of soils, are performed on typical samples (JGS, 2020). In addition, laboratory seepage tests are performed on remoulded samples using the falling head method (JGS, 2020) in the moulds for one-dimensional consolidation tests (ring diameter $D = 60$ mm, ring height $H_0 = 20$ mm). The collected samples, loosened and remoulded in plastic bags, are filled into the moulds under the original water contents. The samples are then submerged in water and deaired in a vacuum chamber for at least 12 h. The saturated samples are consolidated for around 24 h under the stress corresponding to the depths where they were collected, assuming that the remolded samples replicate in-situ densities under the stress. A minimum stress of 19.6 kPa (corresponding to 1 m depth in the ground) is exerted even if the samples are collected in depths shallower than 1 m. Falling head seepage tests are performed after the consolidation, starting from an initial head difference of 600 mm. More details about the tests can be found in Zhang (2024).

3. Field surveys around R 38.9 k of the Kokai River

To reveal the hydraulic characteristics of natural levee sediments, as a case study, a series of field surveys was conducted around R 38.9 k (right bank, 38.9 km measured from the meeting point with the Tone River) of the Kokai River in Japan.

3.1. Layout of the field surveys

Starting from the mountainous area in Tochigi Prefecture, the Kokai River flows through Tochigi and Ibaraki Prefectures, finally joining the Tone River in Tone City (MLIT, 2019). According to the map provided by GSI (2024) in Fig. 6, the lands on the protected side of the river levee along R 38.0 ~ 39.0 k of the Kokai River, in Tategata, Joso City, Ibaraki Prefecture, are taken as the potential target of this study. The natural levees in yellow in the Landform Classification Map for Flood Control (Fig. 6 (a)) correspond to the green wheat farms in the aerial photo (Fig. 6 (b)), compared to the back swamps corresponding to the grey rice paddies. It was confirmed by Sadakata (1972) that the natural levee sediments distributed within 1 m below the ground surface in Tategata consisted of sandy to sandy clay, which may have been deposited before the middle 10th century by the ancient Kinu River (Yamamoto, 2010).

To decide the location of the detailed field surveys, preliminary surveys were conducted between January and March 2024 by performing sounding tests and digging trial pits. In the preliminary surveys, the five levels to describe

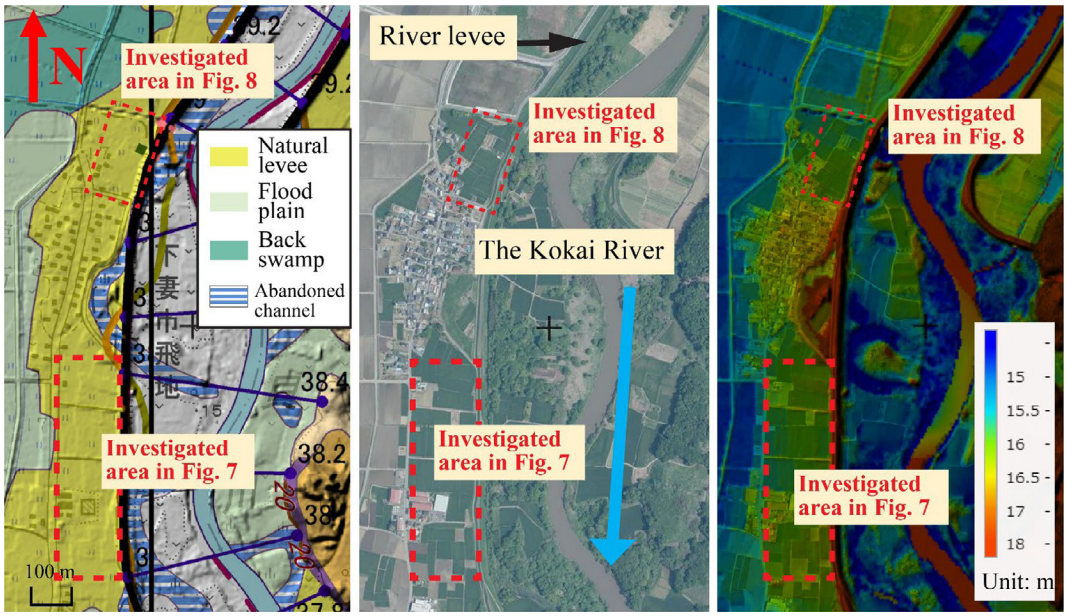

Fig. 6. Classification of landforms (a), aerial photo (b), and elevation map (c) along the R 38.0 ~ 39.0 k of the Kokai River. (after GSI, 2024).

the penetrating resistance (Fig. 4) were not fully set up. Thus, the soil was roughly distinguished by "sandy" soil and "clayey soil" based on the general "hard" and "soft" descriptions of the penetrating resistance during the sounding tests. Soil profiles interpreted by the sounding tests are illustrated in Figs. 7 and 8. The PublicX and PublicY in the figures correspond to the coordinates in the Plane Rectangular Coordinate System of Japan (GSI, 2023), in which the PublicX coordinates point towards the north, while the PublicY coordinates towards the east.

A thick and soft clayey layer overlays a sandy layer in the southern area of Tategata along the R 38.0 ~ 38.4 k of the Kokai River (Fig. 7). Although the area is categorised as natural levees (Fig. 6 (a)), the thick and homogeneous clayey materials are possibly the sediments filling the abandoned channels. In the northern area of Tategata along the R 38.8 ~ 39.0 k of the Kokai River (Fig. 8), a clayey layer with a thickness of 2 ~ 3 m overlays a sandy layer, similar to the cases in the southern part. Different from the southern area, multiple hard-to-firm layers, with several to tens of cm thicknesses, are identified at depths of around 1 ~ 2 m from the ground surface. These laminar structures of fine and coarse materials correspond to the typical characteristics of natural levee sediments (Yamaguchi et al., 2006). Considering the historical leakage events around the Tategata area during the floods due to Typhoon No. 10 on 5th August 1986 (Ishige Town Hall, 1986) and during the tropical storm in August 1988 (Shimodate River Office, 1988), the laminar structures are likely to be the natural levee sediments related to the underseepage problems.

Based on the results from the preliminary surveys, a detailed survey was conducted at R 38.9 k of the Kokai River between March and April of 2024. To reveal the heterogeneity of the natural levee sediments, as shown in Fig. 9(a), sounding tests were concentratedly performed around the "o" spot in Fig. 8, where a leakage event occurred during the flood in 1986. Restricted by the accessibility to the farm, seven sounding tests ("o1" to "o7") were performed near the toe of the levee, in the direction parallel to the levee (the X direction), with a spacing of around 2 m; one sounding test ("z") was performed around 8 m from the toe of the levee (the Y direction); 3 more sounding tests ("n1" to "n3") were performed around the "n" spot in Fig. 8. As shown in Fig. 9 (b), the in-situ seepage tests were conducted around the "o" spot (8 tests in 5 auger holes) and the "n" spot (13 tests in 7 auger holes) in Fig. 8, at a depth of 0.4 ~ 1.6 m from the ground surface. Samples were also collected from the auger holes for observation and grading tests (JGS, 2020).

3.2. Results and discussions

Around R 38.9 k of the Kokai River, through the detailed surveys by the sounding tests and observations on the samples from the auger holes, from the ground surface to a depth of around 5 m, five types of depositional facies, are identified in the ground (Table 1). As illustrated in the example in Fig. 3, identification of depositional facies is mainly based on the 5-level descriptions of the penetrating resistance summarised in Fig. 4 ("vs" to be Ac facies, "s" to be Asc facies, "f" and "h" to be Acs facies, and "vh" to be As facies). The Bc facies are regarded as the continuously distributed soft layer near the ground surface with relatively large vane shear resistance, judged subjectively by the authors. Due to the ambiguous definition of the Bc facies, some Acs and Asc facies in the shallow portion may be classified as Bc facies, leading to an over-

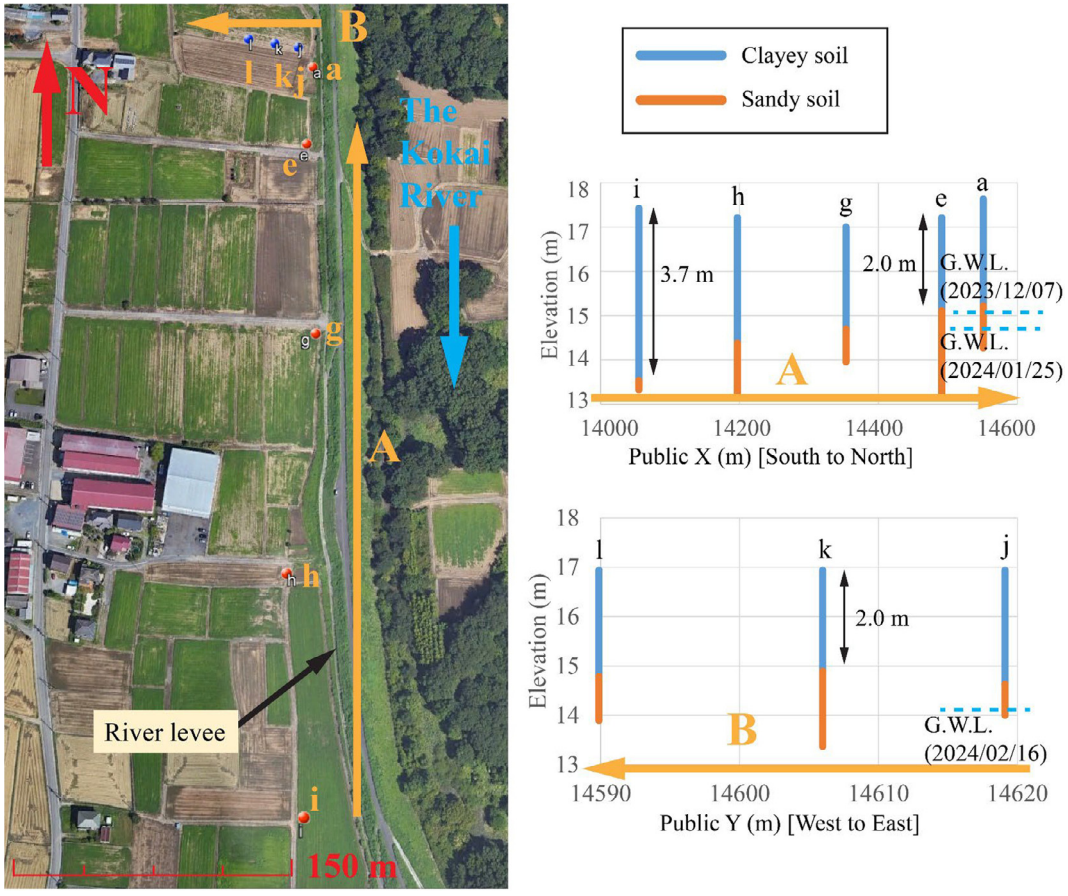

Fig. 7. Soil profiles interpreted by sounding tests along R 38.0 ~ 38.4 k of the Kokai River. (based on Google Earth, May 2024).

estimation of the thickness of Bc facies. The commonly used symbols for soil layers in Japan are applied, where "B" stands for surface soil, "A" stands for alluvium, "c" stands for cohesive soil, "s" stands for cohesionless soil, "sc" stands for cohesive soil mixed with cohesionless contents, and "cs" stands for cohesionless soil mixed with cohesive contents. Among the five kinds of depositional facies, the Asc facies and the Acs facies, with the laminar structures at a depth of around 0.7 ~ 1.8 m from the ground surface in the vicinity of spots "o1" to "o7" and at a depth of around 0.4 ~ 1.3 m in the vicinity of spot "n", are identified as the natural levee sediments.

In every spot of the sounding tests, the classification of depositional facies along the depth is estimated at every 5 cm. By aligning the results around spots "o1" to "o7" and around spot "n", two-dimensional ground profiles can be obtained (Fig. 10). The locations of the auger holes, where the GP tests and soil samplings are performed, are also illustrated in the figure. From the shallow portion to the deep portion, it is found that:

1. The Bc facies, the surface soil disturbed by farming activities, is distributed to a depth of around 0.5 ~ 0.7 m from the ground surface in the vicinity of spots "o1" to "o7" and to a depth around 0.2 ~ 0.5 m in the vicinity of spot "n". Roots, insects, and rubbish are observed in the collected samples.
2. The Asc and Acs facies sandwich each other at a depth of around 0.7 ~ 1.8 m in the vicinity of spots "o1" to "o7" and around 0.3 ~ 1.3 m in the vicinity of spot "n", forming laminar structures. The laminar structures, the depth of the layer, and the grain size distributions to be shown in the following paragraphs, all indicate the distribution of natural levee sediments. The portions, likely related to the leakage events in 1986, are focused on in the following discussions.
3. The clayey Ac facies and the Asc facies below distribute from a depth of around 2 m in the vicinity of spots "o1" to "o7". The very fine material likely comes from the sediments filling the abandoned channels. Considering the existence of the continuously distributed impermeable clayey layer, the coarse materials below the Ac facies (below 2 m from the ground surface) are unlikely to be related to the leakage events.
4. The coarse As facies and the Acs facies above, distributed from a depth of around 4 m in the vicinity of spots "o1" to "o7", are likely to be bed materials of ancient channels.

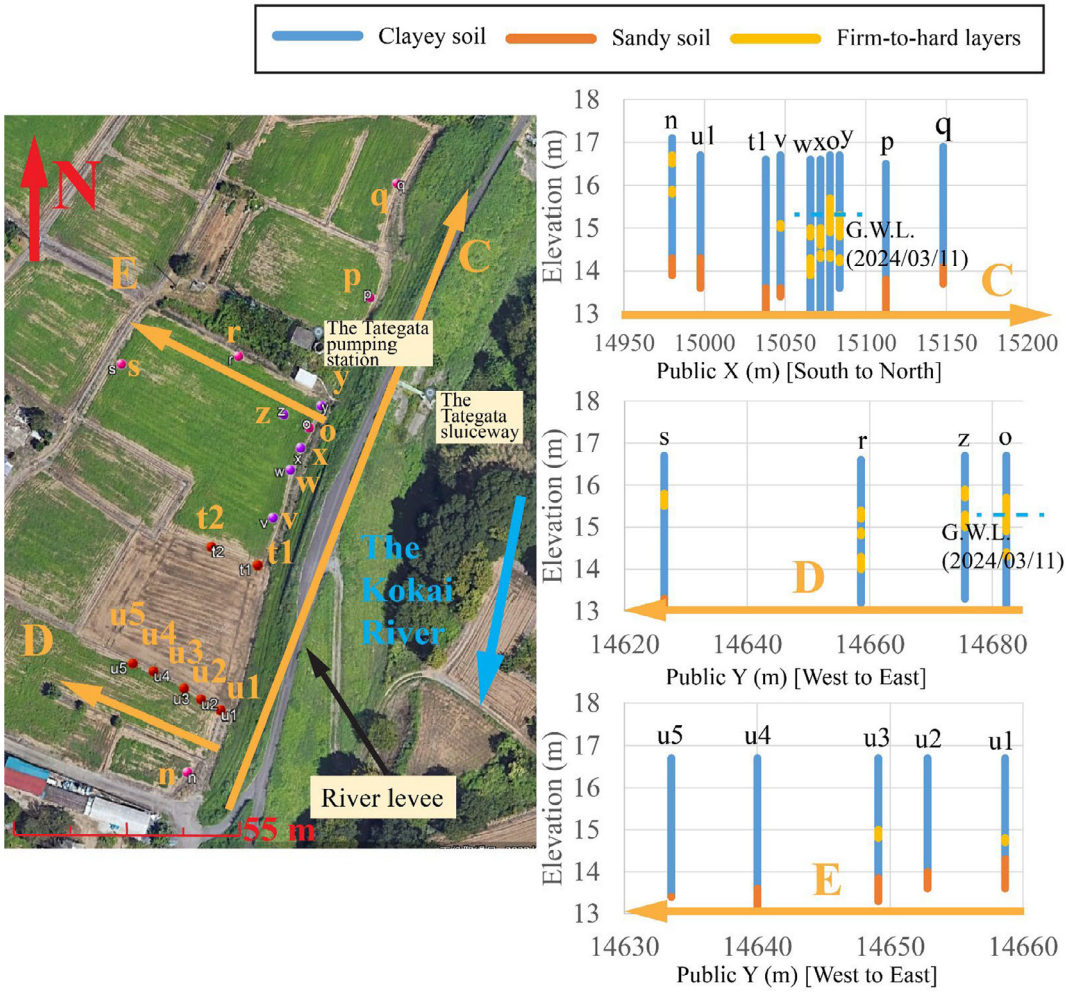

Fig. 8. Soil profiles interpreted by sounding tests along R 38.8 ~ 39.0 k of the Kokai River. (based on Google Earth, May 2024).

5. Compared to the soil profiles around spots "o1" to "o7", the soil profiles around spot "n" are more complex and discontinuous. The clayey contents at a depth of around 1.3 ~ 2.5 m in spots "n" and "n2" are not consistent with the relatively thick Acs facies in the same depth in spots "n1" and "n3". The confusing soil profiles may be related to the meandering ancient channels adjacent (Fig. 6(a)).

The difference between the depositional facies is further illustrated in the grain size distributions of the collected samples (Fig. 11). For comparison, the grain size distributions of the sand dunes (MLIT, 2016) and natural levees (Sato, 2016) along the Kinu River are also plotted in the figure. Among the depositional facies, details about the Asc and Acs facies are summarised in Table 2. It is found that:

1. Variance exists among the grain size distributions of the samples of the same depositional facies, which results in the variance in hydraulic conductivities (Fig. 12).
2. Partially due to the abovementioned variance, the Asc and Acs facies are not distinctively different. The Asc facies are slightly coarser than the Acs facies. Although the Asc and Acs facies have similar grain size distributions (and also similar hydraulic conductivities as mentioned in the following paragraphs), the two facies are distinguished as different depositional facies, supported by the apparent difference in the penetrating resistance in sounding tests, and the visual observation and tactile sense recorded at the site.
3. The Acs facies in the targeted area have grain size distributions similar to the natural levee sediments in the Kinu River, which are obviously finer than the aeolian sand dune sediments in the Kinu River.

Distributions of the hydraulic conductivities of different facies measured by the in-situ seepage tests (Fig. 12) and the statistical characteristics in the natural levee sediments (Table 3) are the most significant concerns in this study. For comparison, the hydraulic conductivities measured by the laboratory seepage tests are also plotted in

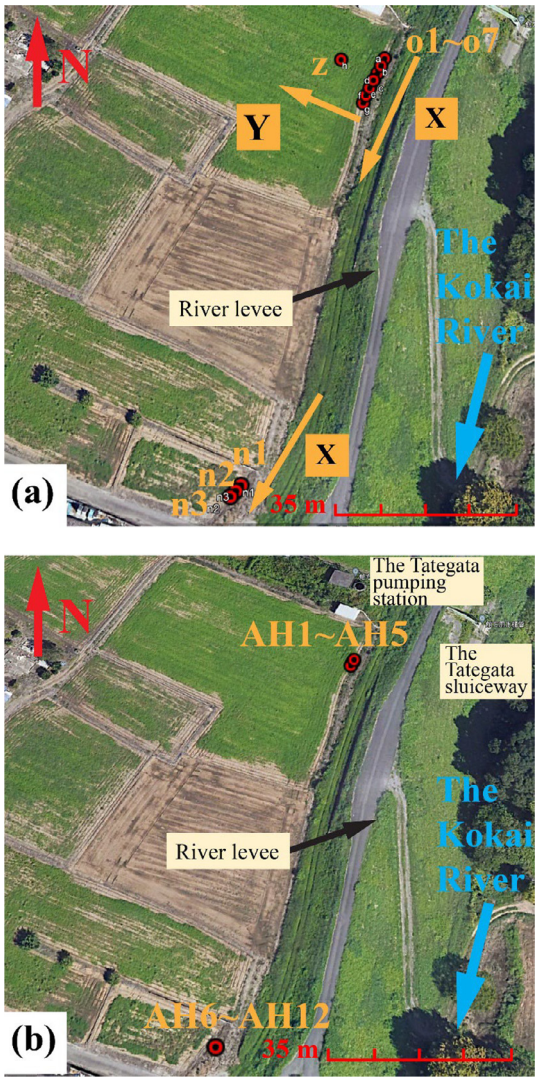

Fig. 9. (a) Sounding tests and (b) GP tests conducted around R 38.9 k of the Kokai River. (based on Google Earth, May 2024).

Fig. 12. In each type of depositional facies (in each column), the pairs of circles and crosses in the same colours (except the ones in black) indicate that the two data are measured at the same depth in the same auger hole. All the hydraulic conductivities are converted to the values at 15 °C. It is found that:

1. A relatively large variance exists in hydraulic conductivities estimated by the GP and laboratory seepage tests in the same depositional facies. Possible causes of the variance include the deviations in classifying the depositional facies, variance in the grain size distributions (Table 2 and Fig. 11), heterogeneity in the same depositional facies, macro-pores in the soil, and errors in the seepage tests.
2. Contrary to expectation, the coarse Acs facies have a slightly lower mean hydraulic conductivity than the finer Asc facies. Possible explanations for the contradictory findings include: (1) The fine contents, which are high in both Asc and Acs facies, determine the hydraulic conductivity rather than the coarse contents; (2) besides the grain size distribution, hydraulic conductivity is also related to the in-situ density, which remains unknown in the study; (3) in the unsaturated zone, shrinking cracks and fissures are more likely to be developed in the more cohesive Asc facies; (4) deviations are included in classifying the depositional facies.
3. Estimations by the GP tests are generally comparable to the measurements by the laboratory seepage tests. Despite the difficulty in defining a "true hydraulic conductivity", the estimations by the GP tests and the laboratory seepage tests are generally consistent. A noticeable deviation exists in the estimation for the clayey Ac facies, where the abnormally high hydraulic conductivity measured by the laboratory seepage test may be related to the leakage around the mould ring or the fissures induced during the preparation of the

Table 1
Details of the five kinds of depositional facies in the targeted area. (Natural levee sediments are highlighted in yellow).

Symbols	Soil naming used in site	Formation	Penetrating resistance [vane shear resistance (N•m)]	In-situ hydraulic conductivity (m/s) [num of tests]
Bc	Silty loam	Surface soil disturbed by farming	Generally soft, but may be affected by roots, gravels, or rubbish. [2 ~ 3]	Around 1.0E-06 [2]
Asc	Silt	Muddy portion of the natural levee	Soft, can be easily penetrated. [1 ~ 3]	Around 4.0E-06 [6]
Acs	Silty sand	Sandy portion of the natural levee	Firm to hard, can be penetrated with the help of rubber hammer. [1 ~ 2.5]	Around 1.0E-06 [12]
Ac	Clay	Fine materials filling the abandoned channels	Very soft, can be penetrated without much effort. [1 ~ 2]	< 1.0E-09 [1]
As	Sand with fine content	Coarse bed materials	Very hard, can be barely penetrated by rubber hammer. [1 ~ 2]	–

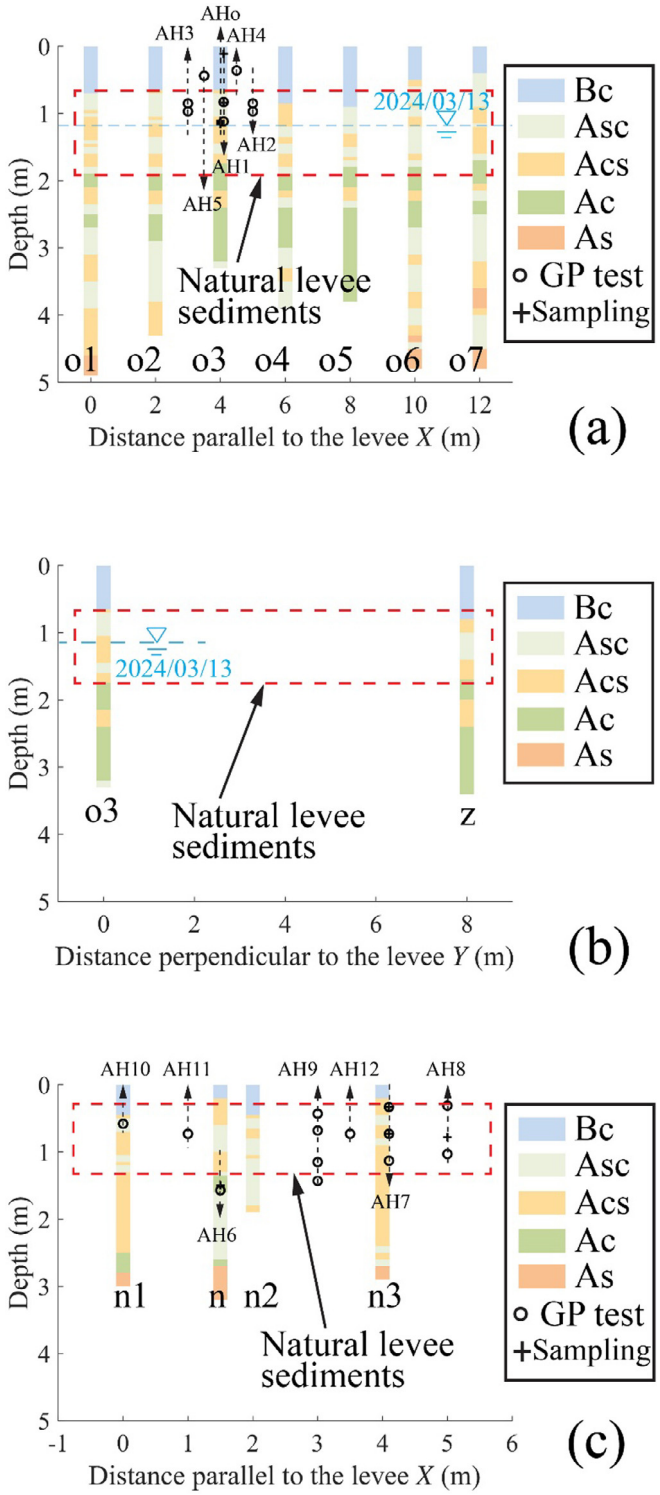

Fig. 10. (a) Distributions of the depositional facies in the direction parallel to the levee around the "o" spot, (b) in the direction perpendicular to the levee around the "o" spot, and (c) in the direction parallel to the levee around the "n" spot.

remoulded sample. No data is estimated by the GP test in the As facies, given that the As facies are distributed under the groundwater level.

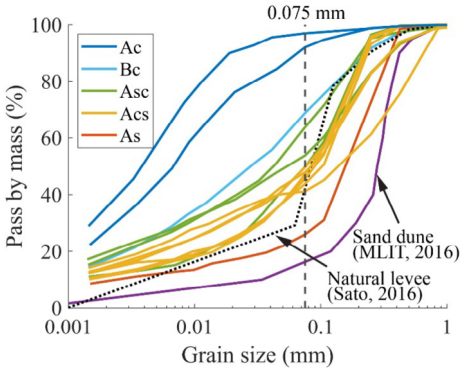

Fig. 11. Grain size distributions of the samples from different depositional facies.

4. The expected highly permeable layer in the natural levee sediments is not found. Given the variance in the data, the Asc and Acs facies generally have similar hydraulic conductivities in the order of E-06 m/s.

4. Modelling the natural levee sediments by geostatistical method

In Section 3, the field surveys attain quantitative data about the hydraulic characteristics of natural levee sediment. For the final goal of risk evaluations against piping, numerical depositional facies models based on the field survey are needed. As mentioned in Section 2, the facies model can better reflect the discrete facies transitions and the geological structures in the ground than the continuous models. In this study, the spatial distributions of lithologic facies are generated by geostatistical methods (Baecher & Christian, 2005), into which mean values of hydraulic conductivity of each lithologic face are assigned (Fogg, 1986). Nonparametric approaches are applied to realise discontinuous heterogeneity, including indicator Kriging (Solow, 1986) and indicator simulations (Ritzi et al., 1994).

4.1. Variogram analysis

Variogram analysis is a common practice to reveal the spatial correlations from the data of the sounding tests (Soulie et al., 1990; Davis et al., 1993; Weerts & Bierkens, 1993). First, indicator random functions are defined for each kind of depositional facies (Bastante, 2008)

$$I(\boldsymbol{u};k)=\begin{cases}1, & \text{if } Z(\boldsymbol{u})\in k\\ 0, & \text{otherwise}\end{cases} \tag{2}$$

where $\boldsymbol{u}$ is spatial locations; Z is a property of the soil; and $k = 1, 2, 3, \ldots$ is the categories.

This study focuses on the natural levee sediments inside which the Asc and Acs facies form laminar structures. As a result, Z corresponds to the classification of depositional

Table 2
Soil properties of the Asc and Acs facies in the natural levee sediments.

Depositional facies	Asc	Acs
Soil Classification based on JGS (2020)	Sandy fine-grained soil (FS)	Sand of fine fraction nature (SF)
Fine content (%)	50 ~ 60	40 ~ 50
D_{20}(mm)	0.002 ~ 0.012	0.004 ~ 0.015
Hydraulic conductivity by Creager's method (Creger et al., 1945) (m/s)	E-09 ~ E-07	E-08 ~ E-07

facies; $k = 1$ and 2 correspond to the Acs and Asc facies. For a typical kind of depositional facies, the function output 1 is only if a specific location is classified as that kind of depositional facies. Because only two types of depositional facies are focused on in the study, the random functions become Bernoulli-distributed.

With the defined indicator random functions, experimental semi-variograms are calculated from the sounding test data. Semi-variogram is a widely used parameter to describe spatial correlation, defined by (Johnson & Dreiss, 1989; Johnson, 1995):

$$\gamma(\boldsymbol{\delta}) = \tfrac{1}{2}E\left[\{I(\boldsymbol{u}+\boldsymbol{\delta}) - I(\boldsymbol{u})\}^2\right] \quad (3)$$

where γ is the semi-variogram, E is the expectation, and $\boldsymbol{\delta}$ is the spatial lag.

In this study, the R package "gstat" ver 2.1-1 (Pebesma, 2004; Gräler et al., 2016) is applied in the calculations of experimental semi-variograms, interpolations of the variogram models, indicator Kriging, and indicator simulations in the following paragraphs.

Based on the distributions of the Acs facies around the "o" spot in the depth of around 0.7 ~ 1.8 m (Fig. 10 (a)),

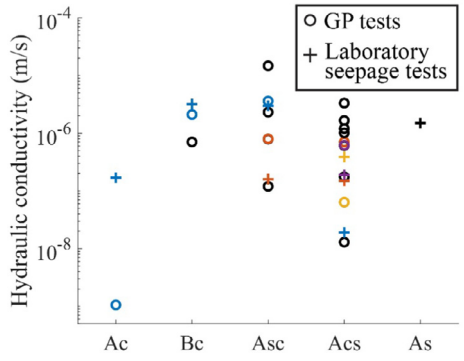

Fig. 12. Hydraulic conductivities of different depositional facies measured by the GP tests and the laboratory seepage tests. (the pairs of circles and crosses in colour indicate that the two data measured at the same depth in the same auger hole).

Table 3
Summary of the statistical characteristics of the in-situ hydraulic conductivity in the natural levee sediments.

Depositional facies [num of data]	Mean (m/s)	Standard deviation (m/s)	Coefficient of variance (*COV*)
Asc [6]	3.7E-06	5.1E-06	1.4
Acs [12]	9.7E-07	8.9E-07	0.91

experimental semi-variograms in the vertical direction and the direction parallel to the levee (the X direction) are calculated for the Acs facies (Fig. 13). The experimental semi-variograms are plotted in black dots; the variogram models interpolated by the spherical model (Mulla & McBrantney, 2001) are plotted in solid lines. Because of the Bernoulli properties of the indicator functions, the experimental semi-variograms and variogram models of the Asc facies are exactly the same as the ones of the Acs facies.

As illustrated in Fig. 13 (a), a typical experimental semi-variogram increases with the increasing lag distance until a constant value is reached. The nugget is the deviation of the semi-variogram from zero in zero lag, which is related to the ground's micro-heterogeneity or measurement errors. The constant value that the semi-variogram reaches, called the sill, is associated with the standard deviation of the random function. The lag distance for the semi-variogram to stabilise, named range, is related to the mean dimension of the clusters. In this case, the range value in the vertical direction is associated with the mean thickness of the Acs facies; the range value in the X direction is related to the mean length of the Acs facies in the horizontal direction parallel to the levee. It is noticeable that in the "gstat" package, the same nugget and sill value are assumed for the variogram models in different directions, while anisotropy is described by different range values in different directions (which is called geometric anisotropy, compared to zonal anisotropy assuming different nuggets, sill values, and range values in different directions) (Mulla & McBratney, 2001). As a result, the variogram models are interpolated using the data in the two directions together. Because of the difference in the abundance of the data in the two directions, good interpolation is ensured in the vertical direction, while considerable uncertainty remains in the horizontal X direction. The limitation is determined by the property of sounding tests, which provide rich data in the vertical direction but are restrained by time and cost, and the accessibility to private lands in the horizontal direction. Despite the deviation, the interpolated variogram models are applied to the indicator Kriging and the indicator simulations in the following.

4.2. Indicator Kriging and indicator simulations

Kriging is a widely applied method to realise spatial best linear unbiased prediction in unsampled spots based on sampled data (Cressie, 1990). Based on the binomial

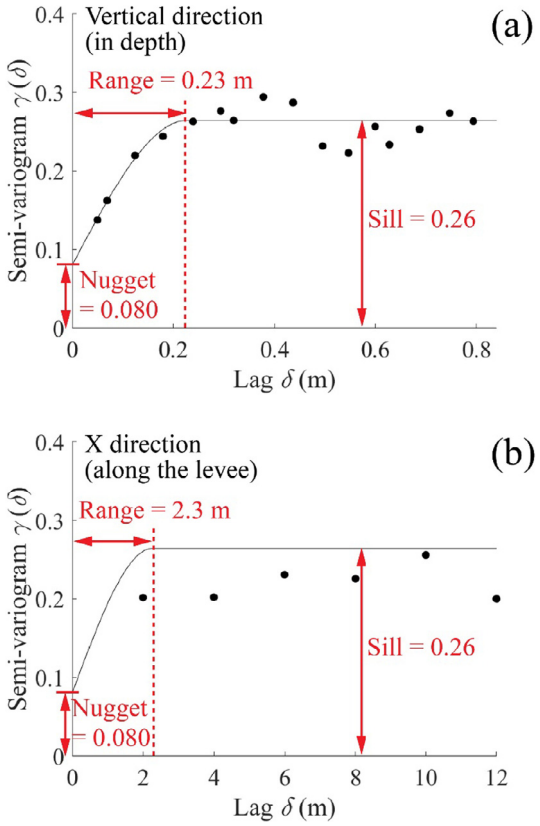

Fig. 13. Experimental semi-variograms and variogram models of the Acs facies in the vertical direction (a) and X direction (b).

characteristics of the indicator random functions (Journel, 1983), nonparametric distributions of depositional facies can be generated by indicator Kriging (Anderson, 1997):

$$\begin{aligned} E[I(\boldsymbol{u};k)] &= 1 \cdot Prob\{Z(\boldsymbol{u}) \in k\} + 0 \cdot Prob\{Z(\boldsymbol{u}) \notin k\} \\ &= Prob\{Z(\boldsymbol{u}) \in k\} \end{aligned} \tag{4}$$

According to Eq. 4, the expectation of the indicator random function equals the probability of the existence of a certain kind of depositional facies. Therefore, generating the distribution of depositional facies is possible by kriging the indicator random function. By applying ordinary Kriging, this is calculated by:

$$I_K^*(\boldsymbol{u}) = \sum_{\alpha=1}^{N} \lambda_\alpha(\boldsymbol{u}) \cdot I(\boldsymbol{u}_\alpha) \tag{5}$$

where I_K^* are the Kriged values; $\alpha = 1, \ldots, N$ refers to the measured data; the weighting factors λ_α, ensuring the best linear unbiased estimation, are calculated by (Journel, 1983; Nielsen et al., 1986):

$$\begin{cases} \sum_{\alpha=1,\beta=1}^{N} \lambda_\alpha(\boldsymbol{u}) \cdot \gamma(\boldsymbol{u_\alpha} - \boldsymbol{u_\beta}) + \mu(\boldsymbol{u}) = \gamma(\boldsymbol{u} - \boldsymbol{u_\alpha}) \\ \sum_{\alpha=1}^{N} \lambda_\alpha = 1 \end{cases} \tag{6}$$

where μ is the Lagrange factor.

By applying Kriging to the indicator random function of the Acs facies, a contour of the probability of the existence

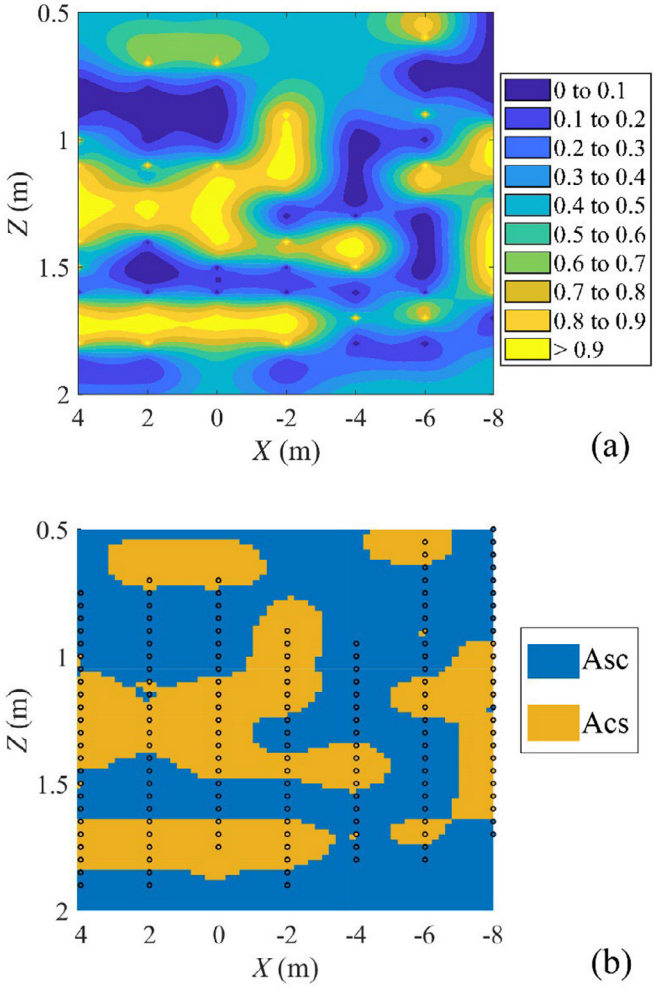

Fig. 14. (a) Contour maps of the kriged indicator random functions of the Acs facies, and (b) a kriged map of the depositional facies in natural levee sediments.

of the Acs facies in a 12 m × 1.5 m two-dimensional space around the "o" spot in Fig. 8 is generated (Fig. 11 (a)). A kriged map of the depositional facies, in other words, a model of the natural levee sediments (Fig. 14 (b)), can then be generated by comparing the probability of existence to the value of 0.5, based on the Bernoulli properties of the indicator functions. The laminar feature of natural levee sediments is reasonably replicated. In the figure, the spots with the sounding test data are marked in black circles, within which the filled colours represent the classification of depositional facies judged by the sounding tests. The colours of the kriged map match the colours in every black circle, indicating that indicator Kriging ensures the consistency of the measured data.

The best spatial estimation can be attained for a tested site by Indicator Kriging. Still, for general discussions on natural levee sediments or risk evaluations involving uncertainties, the generation of infinite realisations is required. By applying the sequential simulation algorithm (Pebesma, 2004), a realisation of unconditional indicator

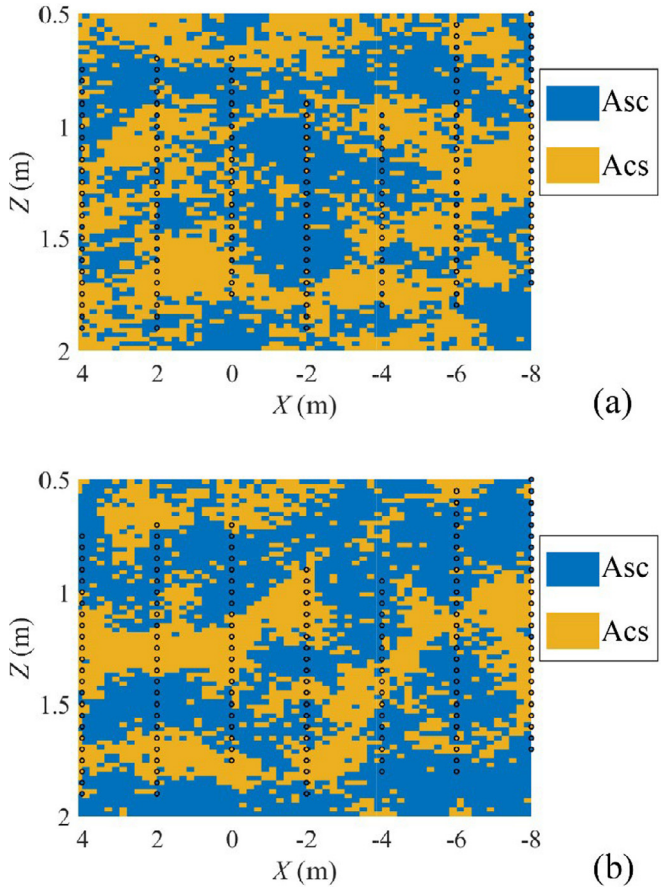

Fig. 15. Examples of a realisation of depositional facies in natural levee sediments by (a) unconditional indicator simulation and (b) conditional indicator simulation.

simulation can be generated (Fig. 15 (a)). The laminar structures of the natural levee sediment are generally replicated. Still, the filled colours in the black circles, referring to the sounding test data, are inconsistent with the simulated results. The spatial structures (the mean, the variance, and the variogram models) are kept, but the information at the exact tested spots is lost.

To keep the consistency with the measured data, conditional indicator simulation can be realised by conditioning the simulation with kriged data (Cressie, 1991; Fenton & Griffiths, 2008; Cáceres et al., 2010):

$$I_{cs}(\boldsymbol{u}) = I_K^*(\boldsymbol{u}) + \left[I_s(\boldsymbol{u}) - I_{sK}^*(\boldsymbol{u})\right] \quad (7)$$

where I_{cs} is the conditional simulation, I_K^* is the kriged value based on the measurement, I_s is the unconditional simulation, and I_{sK}^* is the kriged value based on unconditional simulation at the measured spots. A realisation of conditional indicator simulation is shown in Fig. 15 (b). All the filled colours in the black dots match the simulations, indicating that the consistency of the natural levee sediments' laminar structures and the measurements is maintained.

5. Conclusions

For better maintenance of river levees, knowledge about the heterogeneity related to geological formations is expected to be included in the risk assessment. As a first trial to quantitatively reveal the hydraulic characteristics of natural levees, a study including a field survey and geostatistical modelling was conducted at the site around R 38.9 k of the Kokai River in Japan. It is concluded that:

1. By applying the simple sounding tests, five kinds of depositional facies are identified at the site at around R 38.9 k of the Kokai River. Within 2 m from the ground surface in the targeted site, the laminar structures consisting of silty Asc facies and silty-sand Acs facies are identified as the natural levee sediments.
2. Given the rich fine contents in the natural levee sediments, the expected highly permeable layer cannot be identified. The Acs and Asc facies generally have similar hydraulic conductivities in the order of E-06 m/s. Considering the historical records in the area, the natural levee sediments may lead to leakage events but are unlikely to develop into catastrophic piping failures.
3. Based on the results from the field survey, numerical spatial hydraulic conductivity models of the natural levee sediments can be built by applying geostatistical methods. With the numerical model, quantitative risk assessment against the underseepage of the river levee becomes possible.
4. Only one site is focused on in this research, but the same methodology is expected to be applied to natural levees in other locations in the same river, the natural levees in other flood plains, and other alluvial sediments, including point bars, crevasse splays, or abandoned channels.

CRediT authorship contribution statement

Wenyue Zhang: Writing – original draft, Visualization, Methodology, Investigation, Formal analysis, Conceptualization. **Mai Tabuchi:** Writing – review & editing, Visualization, Investigation. **Tomotaka Yoshikawa:** Writing – review & editing, Investigation. **Akihiro Takahashi:** Writing – review & editing, Supervision, Resources, Investigation, Funding acquisition.

Acknowledgments

The first author acknowledges the Japanese Government (Monbukagakusho: MEXT) scholarship for performing this research during his doctoral study. The experiments in the field were performed under the support of the Kanto Regional Development Bureau, Ministry of Land, Infrastructure, Transport and Tourism, Japan. This work was partially supported by JSPS KAKENHI Grant Nos. 19H02232 and 23K26193.

Appendix A. Information on the GP tests performed in the field survey is summarised in Table A1. The field saturated hydraulic conductivity K_{fs} (m/s) are converted into values at 15 ℃.

Data of the laboratory soil tests performed on the collected samples from the field survey are summarised in Table A2. The d_{20} (mm) is the grain size which 20 % of the samples passed; the $K_{Creager}$ (m/s) is the hydraulic conductivity estimated by Creager's method (Creager et al., 1945); the K_{lab} (m/s) is the saturated hydraulic conductivity estimated by the laboratory seepage test on the remoulded samples. All the hydraulic conductivities are converted into the values at 15 °C.

Table A1

Data of the GP tests from the field surveys.

Closest spot	Auger hole	Date	Case	Depth H (cm)	Depositional facies	K_{fs} (m/s)
o3	AH1	2024/03/13	1-1	90	Asc	2.3E-06
		2024/03/15	1-2	119	Acs	6.1E-07
o3	AH2	2024/03/13	2-1	92	Asc	7.9E-07
		2024/03/14	2-2	104	Acs	7.1E-07
o3	AH3	2024/03/13	3-1	92	Asc	8.0E-07
		2024/03/15	3-2	104	Acs	6.1E-07
o3	AH4	2024/03/15	4-1	43	Bc	7.1E-07
	AH5	2024/03/15	5-1	51	Bc	2.1E-06
n	AH6	2024/03/15	6-1	164	Ac	1.1E-09
n3	AH7	2024/04/11	7-1	40	Acs	6.4E-08
		2024/04/11	7-2	80	Acs	6.2E-07
		2024/04/11	7-3	113	Acs	1.0E-06
n3	AH8	2024/04/11	8-1	38	Acs	1.3E-08
		2024/04/11	8-2	110	Acs	1.8E-07
n2	AH9	2024/04/12	9-1	50	Acs	1.2E-06
		2024/04/12	9-2	75	Acs	1.7E-06
		2024/04/12	9-3	115	Acs	3.3E-06
		2024/04/12	9-4	150	Asc	1.5E-05
n1	AH10	2024/04/12	10-1	65	Asc	3.6E-06
n	AH11	2024/04/12	11-1	80	Asc	1.2E-07
n3	AH12	2024/04/12	12-1	110	Acs	1.7E-06

Table A2

Data of laboratory soil tests on the collected samples.

Sample No.	1	2	3	4	5	6	7
Date (yyyy/mm/dd)	2024/03/11	2024/03/11	2024/03/11	2024/02/16	2024/03/13	2024/03/13	2024/03/14
Closest spot	o	o	o	a	o3	o3	o3
Auger hole	AHo	AHo	AHo	AHa	AH1	AH1	AH1
Depth (cm)	100–120	120–140	150–170	250–280	0–25	80–88	109–119
Depositional facies	Acs	Acs	Asc	As	Bc	Asc	Acs
d_{20} (mm)	0.014	0.010	0.012	0.040	0.0030	0.0023	0.012
$K_{Creager}$ (m/s)	2.1E-07	7.9E-08	1.6E-07	1.7E-06	8.2E-09	5.0E-09	1.1E-07
Fine content Fc (%)	46	47	50	26	69	64	44
In-situ water content w_0 (%)	34.2	32.3	36.6	28.1	31.0	34.5	32.3
Consolidation pressure p (kPa)	19.6			39.2	19.6	19.6	19.6
Void ratio after consolidation e*	0.955			0.937	1.04	0.961	0.910
K_{lab} (m/s)	1.5E-07			1.5E-06	3.2E-06	1.6E-07	1.9E-08

* Calculated from the in-situ water contents, wet densities before consolidation, and settlements during consolidation.

Table A2 (continued)

Sample No.	8	9	10	11	12	13
Date (yyyy/mm/dd)	2024/04/11	2024/04/11	2024/04/11	2024/04/12	2024/03/15	2024/03/11
Closest spot	n3	n3	n1	n3	n	v
Auger hole	AH7	AH7	AH10	AH8	AH6	AHv
Depth (cm)	25–40	65–80	50–70	75–80	143–163	150–180
Depositional facies	Acs	Acs	Asc	Acs	Ac	Ac
d_{20} (mm)	0.0057	0.0052	0.0028	0.0041	< 0.0010	0.0014
$K_{Creager}$ (m/s)	3.8E-08	3.2E-08	7.2E-09	1.5E-08	< 1.0E-9	2.0E-09
Fine content Fc (%)	50	48	54	41	97	92
In-situ water content w_0 (%)	24.0	27.7	28.4	27.0	50.2	42.7
Consolidation pressure p (kPa)	19.6	19.6	19.6			29.4
Void ratio after consolidation e*	– [#]	0.755	0.856			1.20
K_{lab} (m/s)	3.9E-07	1.9E-07	3.0E-06			1.7E-07

[*] Calculated from the in-situ water contents, wet densities before consolidation, and settlements during consolidation.
[#] Data were lost.

References

Anderson, M.P., 1997. Characterisation of geological heterogeneity. In: Dagan, G., Neuman, S.P. (Eds.), Subsurface Flow and Transport: a Stochastic Approach. Cambridge University Press, pp. 23–39.

ASTM International. 2016. Standard Guide for Comparison of Field Methods for Determining Hydraulic Conductivity in Vadose Zone. ASTM D5126-16e1. West Conshohocken, PA: ASTM International, approved 1st July, 2016. https://doi.org/10.1520/D5126-16E01.

Baecher, G.B., Christian, J.T., 2005. Reliability and statistics in geotechnical engineering. John Wiley & Sons.

Bagarello, V., Iovino, M., Reynolds, W.D., 1999. Measuring hydraulic conductivity in a cracking clay soil using the Guelph permeameter. Trans. ASAE 42 (4), 957–964. https://doi.org/10.13031/2013.13276.

Bastante, F.G., Ordóñez, C., Taboada, J., Matías, J.M., 2008. Comparison of indicator kriging, conditional indicator simulation and multiple-point statistics used to model slate deposits. Eng. Geol. 98 (1–2), 50–59. https://doi.org/10.1016/j.enggeo.2008.01.006.

Brierley, G.J., Ferguson, R.J., Woolfe, K.J., 1997. What is a fluvial levee? Sed. Geol. 114 (1–4), 1–9. https://doi.org/10.1016/S0037-0738(97)00114-0.

Brierley, G.J., Fryirs, K.A., 2005. Geomorphology and river management: applications of the river styles framework. Blackwell Publishing.

Cáceres, A., Emery, X., Riquelme, R., 2010. Truncated Gaussian Kriging as an alternative to indicator kriging. Proceeding of 4th International Conference on Mining Innovation, Santiago, Chile, pp. 23–25.

Creager, W.P., Justin, J.D., Hinds, J. 1945. Chap. 16 Soil tests and their utilisation. In: Engineering for Dams, Vol.III: Earth, Rock-fill, Steel and Timber Dams. John Wiley and Sons. pp. 645–654.

Cressie, N., 1990. The origins of Kriging. Math. Geol. 22, 239–252. https://doi.org/10.1007/BF00889887.

Cressie, N., 1991. Statistics for spatial data. John Wiley & Sons.

Davis, J.M., Lohmann, R.C., Phillips, F.M., Wilson, J.L., Love, D.W., 1993. Architecture of the Sierra Ladrones Formation, central New Mexico: Depositional controls on the permeability correlation structure. Geol. Soc. Am. Bull. 105 (8), 998–1007. https://doi.org/10.1130/0016-7606(1993)105%3C0998:AOTSLF%3E2.3.CO;2.

Fenton, G.A., Griffiths, D.V., 2008. 6.5 Conditional simulation of random fields. Risk Assessment in Geotechnical Engineering. John Wiley & Sons, New York, pp. 234–235.

Ferguson, R.J., Brierley, G.J., 1999. Levee morphology and sedimentology along the lower Tuross River, south-eastern Australia. Sedimentology 46 (4), 627–648. https://doi.org/10.1046/j.1365-3091.1999.00235.x.

Filgueira-Rivera, M., Smith, N.D., Slingerland, R.L., 2007. Controls on natural levee development in the Columbia River, British Columbia, Canada. Sedimentology 54 (4), 905–919. https://doi.org/10.1111/j.1365-3091.2007.00865.x.

Fogg, G.E., 1986. Groundwater flow and sand body interconnectedness in a thick, multiple-aquifer system. Water Resour. Res. 22 (5), 679–694. https://doi.org/10.1029/WR022i005p00679.

Fogg, G.E., Noyes, C.D., Carle, S.F., 1998. Geologically based model of heterogeneous hydraulic conductivity in an alluvial setting. Hydrgeol. J. 6, 131–143. https://doi.org/10.1007/s100400050139.

Gräler, B., Pebesma, E.J., Heuvelink, G.B., 2016. Spatio-temporal interpolation using gstat. R J. 8 (1), 204–218 https://journal.r-project.org/archive/2016/RJ-2016-014/RJ-2016-014.pdf.

Geospatial Information Authority of Japan (GSI). 2023. An easy introduction on the Plane Rectangular Coordinate System (In Japanese). https://www.gsi.go.jp/sokuchikijun/jpc.html.

GSI. 2024. About the Landform Classification Map for Flood Control (In Japanese). Retrieved from https://www.gsi.go.jp/bousaichiri/fc_index.html.

Hayashi, K., 2008. Development of the Surface-Wave Methods and its Application to site Investigation. Kyoto University (PhD thesis).

Ishige Town Hall, 1986. Breaching of the Kokai River (In Japanese). Bulletin in Ishige 257 https://joso.ibaraki-ebooks.jp/actibook_data/acv-joso_198608_i257/HTML5/pc.html#/page/1.

Itsukushima, R., 2018. Countermeasures against floods that exceed design levels based on topographical and historical analyses of the September 2015 Kinu River flooding. J. Hydrol.: Reg. Stud. 19, 211–223. https://doi.org/10.1016/j.ejrh.2018.10.001.

The Japanese Geotechnical Society (JGS), 2017. Method for determination of field saturated hydraulic conductivity above water table. Maruzen Publishing.

JGS. 2020. Japanese Standards and Explanations of Laboratory Tests of Geomaterials – The First Revised Edition. JGS.

Japan Institute of Country-ology and Engineering (JICE). 2012. Guideline for the structural evaluation of levees (In Japanese). Retrieved from http://www.jice.or.jp/cms/kokudo/pdf/tech/material/teibou_kouzou02.pdf.

Johnson, N.M., Dreiss, S.J., 1989. Hydrostratigraphic interpretation using indicator geostatistics. Water Resour. Res. 25 (12), 2501–2510. https://doi.org/10.1029/WR025i012p02501.

Johnson, N.M., 1995. Characterisation of alluvial hydrostratigraphy with indicator semi-variograms. Water Resour. Res. 31 (12), 3217–3227. https://doi.org/10.1029/95WR02571.

Journel, A.G., 1983. Nonparametric estimation of spatial distributions. J. Int. Assoc. Math. Geol. 15, 445–468. https://doi.org/10.1007/BF01031292.

Kanning, W., 2012. The weakest link: spatial variability in the piping failure mechanism of dikes. Delft University of Technology (PhD thesis).

Kuroki, T., Shinagawa, S., 2018. Damages caused by Kanto-Tohoku heavy rainfall in September 2015 and Micro-landform of the Kinu River (In Japanese). Bulletin Univ. Teach. Educat. Fukuoka Part II, Social Sci. 67, 1–11.

Liang, Y., Yeh, T.C.J., Wang, Y.L., Liu, M., Wang, J., Hao, Y., 2017. Numerical simulation of backward erosion piping in heterogeneous fields. Water Resour. Res. 53 (4), 3246–3261. https://doi.org/10.1002/2017WR020425.

MacDonald, A.M., Maurice, L., Dobbs, M.R., Reeves, H.J., Auton, C.A., 2012. Relating in situ hydraulic conductivity, particle size and relative density of superficial deposits in a heterogeneous catchment. J. Hydrol. 434, 130–141. https://doi.org/10.1016/j.jhydrol.2012.01.018.

Martin, S.M., Dunbar, J.B., Corcoran, M.K., and Schmitz, D.W. 2017. ERDC/GSL TR-17-12 Geologic controls of sand boil formation at Buck Chute, Mississippi. Geotechnical and Strucures Laboratory, Engineer Research and Development Center, US Army Corps of Engineers.

Ministry of Land, Infrastructure, Transport and Tourism (MLIT). 2007. Design Guideline for Levees (In Japanese). Retrieved from https://www.mlit.go.jp/river/shishin_guideline/bousai/gijyutukaihatu/pdf/teibou_sekkei.pdf.

MLIT. 2016. Materials for the 4th Technical Commetti on the Kinu River Dike: Report for the detailed investigation of the leakage spots in the levees. Retrieved from https://www.ktr.mlit.go.jp/ktr_content/content/000642509.pdf.

MLIT. 2019. About the current situations and problems of the Kokai River (In Japanese). Retrieved from https://www.ktr.mlit.go.jp/ktr_content/content/000738148.pdf.

Mulla, D.J., McBratney, A.B., 2001. Soil spatial variability. In: Warrick, A.W. (Ed.), Soil Physics Companion. CRC Press, Boca Raton, pp. 343–377.

Negrinelli, G., Van Beek, V.M., Ranzi, R., 2016. Experimental and Numerical Investigation of Backward Erosion Piping in Heterogeneous Sands. CRC Press.

Nielsen, D.R., Warrick, A.W., Myers, D.E., 1986. Geostatistical methods applied to soil science. Methods Soil Anal.: Part 1 Phys. Mineral. Methods 5, 53–82. https://doi.org/10.2136/sssabookser5.1.2ed.c3.

Pebesma, E.J., 2004. Multivariable geostatistics in S: the gstat package. Comput. Geosci. 30 (7), 683–691. https://doi.org/10.1016/j.cageo.2004.03.012.

Polanco-Boulware, L., Rice, J.D., 2017. Reliability-based three-dimensional assessment of internal erosion potential due to crevasse splays. J. Geotech. Geoenviron. Eng. 143 (4). https://doi.org/10.1061/(ASCE)GT.1943-5606.0001596 04016111.

Public Works Research Institute (PWRI). 2010. Research on the investigation methods on the hydraulic characteristics of the foundation of levees (In Japanese). Retrieved from https://www.pwri.go.jp/jpn/results/report/report-project/2010/pdf/pro-2-3.pdf.

Reynolds, W.D., Elrick, D.E., 1987. A laboratory and numerical assessment of the Guelph permeameter method. Soil Sci. 144 (4), 282–299 https://journals.lww.com/soilsci/abstract/1987/10000/a_laboratory_and_numerical_assessment_of_the.8.aspx.

Reynolds, W.D., 2013. An assessment of borehole infiltration analyses for measuring field-saturated hydraulic conductivity in the vadose zone. Eng. Geol. 159, 119–130. https://doi.org/10.1016/j.enggeo.2013.02.006.

Ritzi Jr, R.W., Jayne, D.F., Zahradnik Jr, A.J., Field, A.A., Fogg, G.E., 1994. Geostatistical modeling of heterogeneity in glaciofluvial, buried-valley aquifers. Groundwater 32 (4), 666–674. https://doi.org/10.1111/j.1745-6584.1994.tb00903.x.

River Center of Hokkaido. (Published as Foundation of Hokkaido River Disaster Prevention Research Center, 2004). Countermeasures against leakage of levees (In Japanese). Retrieved from http://www.ric.or.jp/profile/works/kiyou/h1608.pdf.

Robbins, B.A., Griffiths, D.V., Fenton, G.A., 2021. Random finite element analysis of backward erosion piping. Comput. Geotech. 138. https://doi.org/10.1016/j.compgeo.2021.104322 104322.

Sadakata, N., 1972. Formation of the lower Kinu River Floodplain (In Japanese). Geographical Sciences 18, 13–22. https://doi.org/10.20630/chirikagaku.18.0_13.

Sato, H. 2016. Particle size analysis of flood sediment around the dike-broken site in Kinugawa River (In Japanese). In: Proceedings of the General Meeting of the Association of Japanese Geographers, the conference in spring, 2016. The Association of Japanese Geographers. 2016. https://doi.org/10.14866/ajg.2016s.0_100289.

Shimodate River Office. 1988. Application report of the funding for the recovery of the river managed by the national government against the disaster (tropical storm) in August 1988 (In Japanese).

Solow, A.R., 1986. Mapping by simple indicator kriging. Math. Geol. 18, 335–352. https://doi.org/10.1007/BF00898037.

Soulie, M., Montes, P., Silvestri, V., 1990. Modelling spatial variability of soil parameters. Can. Geotech. J. 27 (5), 617–630. https://doi.org/10.1139/t90-076.

Strange, R. C., Corcoran, M. K., Dunbar, J. B., Schmitz, D. 2016. ERDC/GSL TR-16-7. The influences of geologic depositional environments on sand boil development, Tara Wildlife Lodge Area in Mississipi. Geotechnical and Strucures Laboratory, Engineer Research and Development Center, US Army Corps of Engineers. Retrieved from https://apps.dtic.mil/sti/tr/pdf/AD1006973.pdf.

Winkels, T.G., Cohen, K.M., Knaake, S.M., Middelkoop, H., Stouthamer, E., 2021. Geological framework for assessing variability in subsurface piping parameters underneath dikes in the Rhine-Meuse delta, the Netherlands. Eng. Geol. 294. https://doi.org/10.1016/j.enggeo.2021.106362 106362.

Workshop on the Handle Penetrating Stick. 2023a. Manual for the investigation and evaluation using the handle penetrating stick – Commons (draft) (In Japanese). Retrieved from https://dokenbo.org/.

U.S. Army Corps of Engineers (USACE). 2000. Design and Construction of Levees, EM 1110-2-1913. Retrieved from https://www.publications.usace.army.mil/Portals/76/Publications/EngineerManuals/EM_1110-2-1913.pdf.

USACE. 2005. Engineering and design: Design guidance for levee underseepage, ETL 1110-2-569. Retrieved from https://www.mvn.usace.army.mil/Portals/56/docs/engineering/HurrGuide/ETL_1110-2-569_%20DESIGN_GUIDANCE_FOR_LEVEE_UNDERSEEPAGE_May_2005.pdf.

Weerts, H.J., Bierkens, M.F., 1993. Geostatistical analysis of overbank deposits of anastomosing and meandering fluvial systems; Rhine-Meuse delta, The Netherlands. Sedimen. Geol. 85 (1–4), 221–232. https://doi.org/10.1016/0037-0738(93)90085-J.

Yamaguchi, M., Sugai, T., Fujiwara, O., Ogami, T., Ohmori, H., 2006. Stratigraphy of upper Holocene deposits and landform evolution in the Kiso river delta system, central Japan (In Japanese). Quat. Res 45 (6), 451–462. https://doi.org/10.4116/jaqua.45.451.

Yamamoto, K., 2010. Alluvial river: Configuration and dynamics (In Japanese). Gihodo Shuppan Co. Ltd..

Zhang, W., 2024. A study on the hydraulic characteristics of alluvial sediments in river levee systems through field surveys and statistical analysis. Tokyo Institute of Technology (PhD thesis).

Zhang, W., Takahashi, A., 2022. Statistical and parametric studies on natural levees as weak points against leakages in river levees. Geotech. Geol. Eng. 40 (11), 5643–5666. https://doi.org/10.1007/s10706-022-02238-y.

Zhang, W., Takahashi, A., 2024. Assessment of the Applicability of a Constant-Head Borehole Permeameter Test to River Levees. Geotech. Test. J. 47 (2), 846–862. https://doi.org/10.1520/GTJ20230433.